

Long-Distance Indirect Excitation of Nanoplasmonic Resonances

Worawut Khunsin,^{*,†} Björn Brian,[‡] Jens Dorfmüller,[†] Moritz Esslinger,[†] Ralf Vogelgesang,^{*,†} Christoph Etrich,[§] Carsten Rockstuhl,[§] Alexandre Dmitriev,^{*,‡} and Klaus Kern^{†,||}

[†]Max-Planck-Institut für Festkörperforschung, Heisenbergstrasse 1, 70569 Stuttgart, Germany

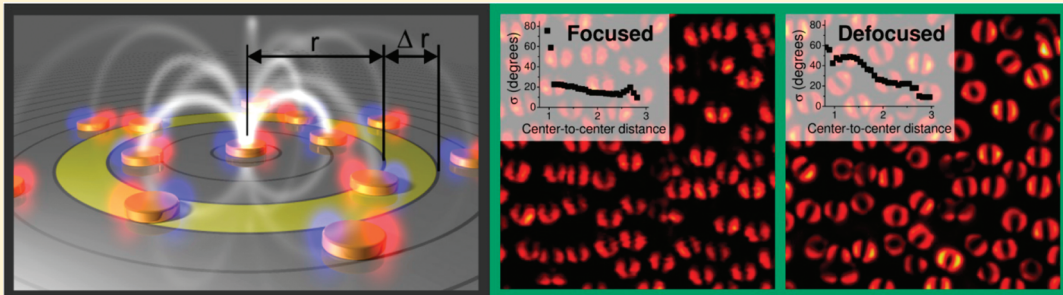
[‡]Department of Applied Physics, Chalmers University of Technology, SE-412 96 Göteborg, Sweden

[§]Institut für Festkörpertheorie und -optik, Abbe Center of Photonics, Friedrich-Schiller-Universität Jena, Max-Wien-Platz 1, 07743 Jena, Germany

^{||}Institut de Physique de la Matière Condensée, École Polytechnique Fédérale de Lausanne, 1015 Lausanne, Switzerland

 Supporting Information

ABSTRACT:



In nanoscopic systems, size, geometry, and arrangement are the crucial determinants of the light-matter interaction and resulting nanoparticles excitation. At optical frequencies, one of the most prominent examples is the excitation of localized surface plasmon polaritons, where the electromagnetic radiation is coupled to the confined charge density oscillations. Here, we show that beyond direct near- and far-field excitation, a long-range, indirect mode of particle excitation is available in nanoplasmonic systems. In particular, in amorphous arrays of plasmonic nanodiscs we find strong collective and coherent influence on each particle from its entire active neighborhood. This dependency of the local field response on excitation conditions at distant areas brings exciting possibilities to engineer enhanced electromagnetic fields through controlled, spatially configured illumination.

KEYWORDS: Amorphous plasmonics, near-field optics, plasmonic localization, near-field coupling, neighbor interaction, hot spot

The beauty of electromagnetic radiation, which can self-perpetuate in vacuum, is that it also interacts with matter. In unstructured bulk matter this interaction is governed solely by material properties, that is, electric permittivity and magnetic permeability. In recent decades, advances in nanofabrication and measurement techniques have revealed fascinating new ways of manipulating the optical response to direct excitation of nanoplasmonic systems by varying size^{1–3} and shape.^{4–6} A prominent second option for controlling plasmonic resonances^{7,8} has been identified in the interparticle distance^{3,9–15} and/or orientation,^{16–18} which has been addressed with the plasmonic dimer (i.e., two-particle system) configurations. In general, dimer systems are conveniently explained within the framework of plasmonic mode hybridization,¹⁹ a successful model that describes the strong coupling via near-field interaction between nanoplasmonic entities in close analogy to concepts from molecular chemistry. Recently, these ideas have been expanded to higher order oligomers, toward what might be called meta-molecular plasmonic systems.^{20–22}

With this Letter, we put forward an amorphous nanoplasmonic system^{23,24} that effectively possesses statistical variation on

the arrangement of nearest neighbors. Contrary to conventional practice of light-matter interaction experiment in which the recorded signal is usually attributed to the object under study, for example, one might refer to “the absorption spectrum” of a certain particle, we show that the excitation strength of a localized plasmonic resonance depends exclusively on the local field of the illumination. This local field, however, depends sensitively on the arrangement of the entire structure that generally comprises many strongly scattering entities. We note that in a recent work by Knight et al.,²⁵ it was shown that spectra of partially integrated differential cross section depend sensitively on excitation and collection angles, even for the same plasmonic particle, and may not be equivalent to the total spectrum. However, for an array of closely spaced plasmonic nanoparticles and due to the short-range interaction of near-field coupling, studies of illumination

Received: March 28, 2011

Revised: May 26, 2011

Published: June 08, 2011

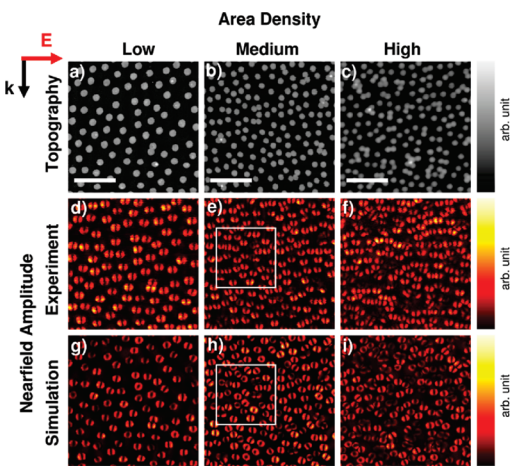


Figure 1. (a–c) AFM topography of the three amorphous nanoplasmonic arrays of nanodisks under investigation, labeled according to nanodisk area density. (d–f) Experimental near-field amplitudes. (g–i) Simulated near-field amplitude of the exact same disk arrangement taken at 20 nm above the sample surface. The excitation wavelength is 897.8 nm. The polarization and the in-plane wave vector of the incident light are indicated on the top-left corner of the figure. White rectangles exemplify the difference in dipole orientation between the experiment and simulation. The scale bars are 1 μm long.

conditions on randomly oriented nanoparticles are only possible in the near field.

We have devised a number of short-range-ordered nanoplasmonic arrays of gold nanodisks with varying density (hence, interparticle distance). They are denoted as low, medium, and high density arrays, respectively. The nanodisks are fabricated using hole-mask colloidal lithography (HCL)²⁶ with nominal diameter D and height h of 190 and 25 nm, respectively (see Methods and Figure S1 in Supporting Information). The local properties of this amorphous structure are analyzed by an apertureless scanning near-field optical microscope (aSNOM)²⁷ with a cross-polarization scheme,^{28–30} complemented by a large-scale finite-difference time-domain (FDTD) simulation that takes the exact details of the array fully into account. aSNOM characterization is performed on extended domains of 10 μm by 10 μm and with a spatial resolution of 20 nm.

Figure 1 shows 3 μm by 3 μm cut-outs for ease of viewing. Panels a, b, and c show atomic force microscopy (AFM) topographs for low-, medium-, and high-density arrays, respectively. The corresponding measured amplitudes of the E_z components of the near field are shown in Figure 1d–f. Clear characteristic dipole oscillations can be readily observed. Furthermore, the in-plane dipole orientations are predominantly dictated by the polarization of the incident wave, but a variation in the dipole orientations exists and is higher for denser arrays. Finally, a variation occurs in dipole excitation strength akin to plasmonic hot spots.³¹ Qualitatively, a similar trend appears in the full-area FDTD simulations. However, a closer look reveals a contrasting difference that is exemplified by the white rectangles highlighted in panels e and h. Noticeably, the simulated dipole orientations show a much wilder fluctuation. A strong difference is already present in the low-density array, the average interparticle distance of which is in the range where near-field coupling becomes negligible and dipole–dipole interaction takes over.³² The observed variation in the dipole orientation suggests a second, more dominating factor governing the characteristics of individual

nanodisks: coherent excitation by scattered field from surrounding neighbors. We also note that due to amorphous nature of our samples the contribution from coherent build-up of scattered light due to ordered arrays³³ can be disregarded.

To quantify the effect of coherent excitation from surrounding neighbors, we consider in-plane dipole moments \mathbf{P} (P_x, P_y) for each nanodisk, extracted from measured or simulated data, and statistically study the coherent interaction in terms of correlations between interparticle distance and dipole orientation with respect to the external excitation (see Supporting Information for details). The results extracted from the measured and corresponding simulated data taking into consideration all the three samples at once are shown in Figure 2a,b, respectively. Further, Figure 2c shows standard deviation plots of the dipole orientations from Figure 2a,b against nearest-neighbor separation between plasmonic nanodisks. Whereas for a center-to-center nearest-neighbor distance of more than about 2.5 times the disk diameter the dipole orientation is close to that of an isolated particle, around $\theta = 0^\circ$, with decreasing interparticle distance the spread in dipole orientations becomes larger and eventually spans the whole interval ($-90^\circ \leq \theta \leq +90^\circ$) for nearly touching and connected dimers (data points left of the red lines in Figure 2a,b). Evidently, the discrepancy between experiment and simulation increases as the nearest-neighbor interparticle spacing approaches zero gap size. It is worth noting that due to the amorphous arrangement of the nanodisks the coupling of the surface charges across particle pairs varies and contains both attractive and repulsive interactions that lead, respectively, to a reduced or enhanced dipole moment of individual particles.¹¹

All else being equal, that is, excitation wavelength, incident angles, and sample topology, a closer look at the excitation condition between experiment and simulation reveals one crucial difference, that is, the “active” or “illuminated” area is smaller in the experiment compared to the full-area illumination in the simulation that is assumed to be excited by a plane wave. Figure 2d shows a schematic of excitation configuration used in the experiment (left) and simulation (right). An important consequence of this difference is that the contribution of the scattered fields from surrounding nanodisks on the response of a particular nanodisk is limited by the illumination spot size in the experiment and the simulated area in the simulation. We note that the statistics on dipole orientation is not affected by a particular choice of incident angle. (see Figure S2 in Supporting Information for details).

To roughly estimate the magnitude of the collective influence from scattered fields from all the surrounding particles that act upon that center particle, we consider the principal composition of the scattered field, \mathbf{E}_{sca} at any particle in the first-order Born approximation, given by a volume convolution of a Green function $\underline{\underline{G}}(\mathbf{r}, \mathbf{r}')$ with $\mathbf{E}_{\text{inc}}(\mathbf{r})$

$$\mathbf{E}_{\text{sca}}(\mathbf{r}) = \int_{V'} \underline{\underline{G}}(\mathbf{r}, \mathbf{r}') \omega^2 \mu_0 \delta\epsilon(\mathbf{r}') \mathbf{E}_{\text{inc}}(\mathbf{r}') d\mathbf{r}'^3 \quad (1)$$

where $\delta\epsilon(\mathbf{r})$ represents scattering centers distributed in space. In free space, the Green propagator is proportional to the inverse of the distance $R = |\mathbf{r} - \mathbf{r}'|$ between the points of cause and effect, $\underline{\underline{G}}(\mathbf{r}, \mathbf{r}') \propto \exp(ikR)/4\pi R$. (The appropriate Green function for a substrate–air interface behaves similarly.) The incoherently integrated effect at the center from any ring area ($A = 2\pi R\Delta r$) of uniformly distributed particles is proportional to the width $|\underline{\underline{G}}(\mathbf{r}, \mathbf{r}')|A \propto \Delta r$, but it does not depend on the ring’s radius R . The incoherent sum also represents the maximum amplitude of

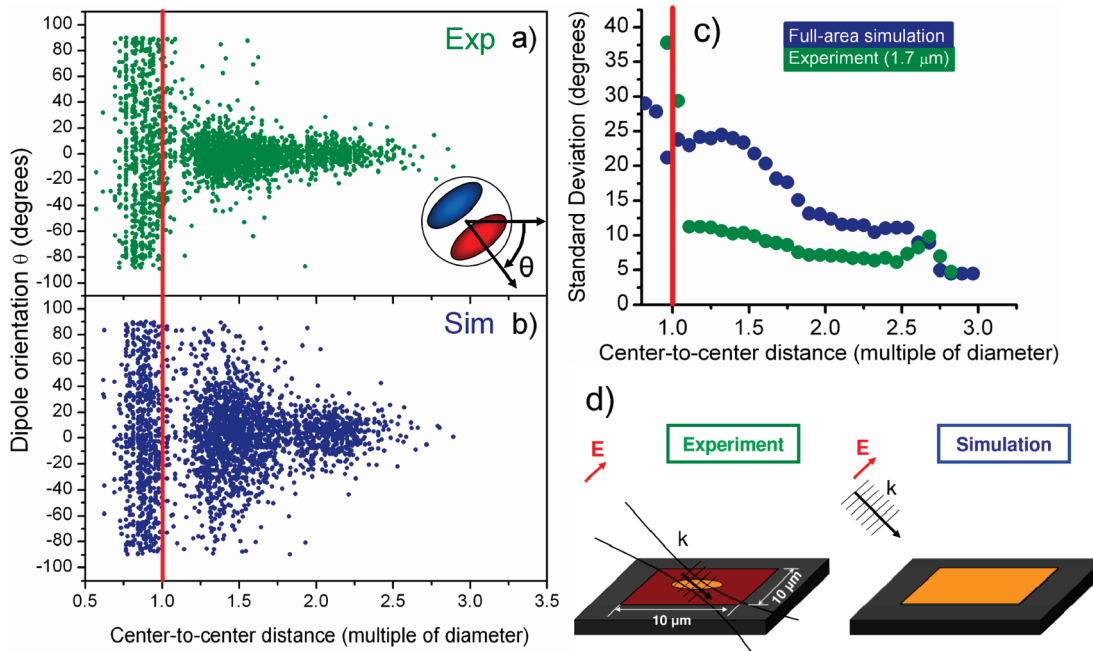


Figure 2. Dipole orientation as a function of nearest-neighbor separation for (a) experiment and (b) simulation. (c) Standard deviation of dipole orientations as a function of nearest-neighbor separation. Simulation assumes plane wave illumination of the entire sample (blue circles) and in the experiment the sample is illuminated with a focus spot size of $1.7 \mu\text{m}$ (green circles). (d) Schematics showing illumination configuration used in the experiment (left) and simulation (right). Polarization and wave vector of the incident light are as indicated. Orange-shaded region represents the illuminated area, dark red is the total measured area (in the experiment), and gray is the unprobed region.

the total field, coherently integrated over the ring area according to eq 1. Thus, whereas a single scatterer contributes to the center field with a magnitude that diminishes inversely with distance, the sum over a ring of randomly arranged scatterers cannot be neglected. Figure 3 illustrates the influence of the scattered fields from neighboring plasmonic nanodisks on the characteristics of the nanodisc in the center. The complete integral in eq 1 may be thought of as the coherent sum of a concentric sequence of such rings covering the excitation spot, each contributing with a similar magnitude, and the total field at the center becomes ever more varied, the larger the number of rings. Consequently, the overall statistical behavior of the sample should strongly depend on the illumination focus size.

Experimentally, different focus spot sizes can be achieved straightforwardly with the use of an iris aperture that controls the illumination beam width (see Supporting Information for details). Plots of standard deviation of dipole orientation distribution are shown in Figure 4 for different spot sizes. It is observed that larger spot sizes indeed yield a wider distribution, which eventually converges with the simulated data at the focus size of about $4 \mu\text{m}$ in diameter. The effect of increasing the spot size is, in fact, 2-fold. First, by increasing the illumination spot size, that is, the orange-shaded area on the left-hand side in Figure 2d, more and more discs contribute to the overall statistics and characteristics of the data being measured. Second, by enlarging the focus spot size, the illumination wavefront becomes more and more plane-wave like, thus mimicking the excitation source used in the simulation.

We show that in addition to neighbor separation controlling the external illumination structure has a profound influence on the optical near fields in nanoplasmonic array, exemplified by the amorphous system of nanodisks. By changing the focus size, we demonstrate that the local field response of individual plasmonic

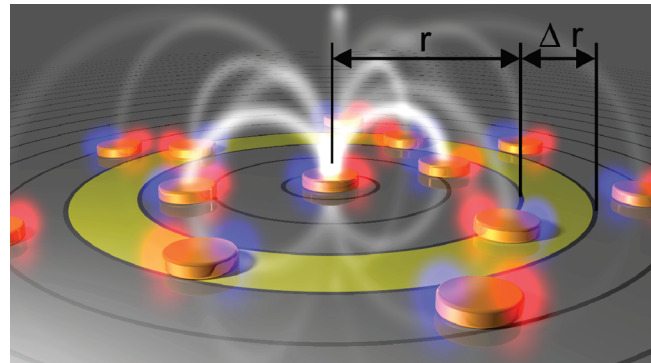


Figure 3. A schematic showing the influence of distant plasmonic scatterers on the characteristics of the center plasmonic nanodisc. The white fuzzy lines portray the scattered fields from surrounding plasmonic nanodisks, which coherently superimpose at the center nanodisc. Red and blue lobes represent the dipole oscillation of the discs.

nanostructures depends very sensitively on illumination condition, essentially establishing a new modality for the excitation of nanoplasmonic systems, what we call long-distance indirect excitation. The ability to vary the local response of a plasmonic entity is of immediate interest to the field of hot-spot and energy concentration engineering with immediate applications, for example, in enhanced Raman scattering spectroscopy. Our work also indicates that the very high-field enhancements achieved in SERS^{34,35} might not have their origin in the very local surrounding,³⁶ but originate from coherent interaction of a larger region. Earlier work on energy localization was based on polarization pulse shaping, which works in the temporal domain,^{37–39}

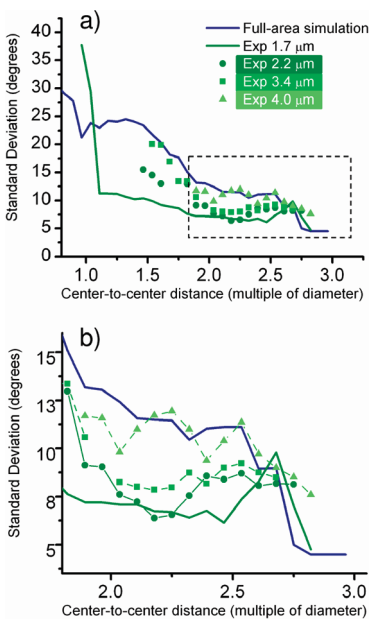


Figure 4. (a) Standard deviation of dipole orientation as a function of center-to-center separation. Full-area FDTD simulation (blue line) and experiment with a focus spot size of $1.7\text{ }\mu\text{m}$ (green line) are the same as those shown in Figure 2c. Measured data obtained from measurements with varying focus spot size are shown in different hues of green as denoted. (b) A zoom-in of the area enclosed by the dashed rectangle in panel (a).

or through the use of purposefully tailored structures.⁴⁰ Recently, the localization control has been achieved in the spatial domain via spatially controlled wavefronts of illumination beam on subwavelength grating,⁴¹ coherent superposition of high-order beams⁴² and spatially tailored phase profiles with strongly interacting metamolecules platform.^{43,44} However, these techniques either rely on sophisticated sample preparation like electron beam lithography or require prior knowledge of the sample's morphology. For the approach presented here, no specially designed structures are needed and the dynamic control of light localization can be achieved at low cost. Our ability to control local response in amorphous plasmonic system can be further enhanced by spatial beam profile modulation and as such is a strong contender as a tool to engineer hot spot formation and light localization.

■ ASSOCIATED CONTENT

Supporting Information. Materials and methods, far-field transmission spectra, calculation of dipoles' orientation, experimental variation of illumination condition, and effect of incident angle on dipoles orientation. This material is available free of charge via the Internet at <http://pubs.acs.org>.

■ AUTHOR INFORMATION

Corresponding Author

*Tel: (W.K., R.V.) +49-711-689-1581; (A.D.) +46-31-772-5177. Fax: (W.K., R.V.) +49-711-689-1662. E-mail: (W.K.) wkhunsin@flkf.mpg.de; (R.V.) r.vogelgesang@flkf.mpg.de; (A.D.) alexd@chalmers.se.

■ ACKNOWLEDGMENT

W.K., J.D., M.E., R.V., C.R., and C.E. thank the Deutsche Forschungsgemeinschaft (SPP1391) and the BMBF (METAMAT)

for financial support. B.B. and A.D. acknowledge support from the Swedish Research Council.

■ REFERENCES

- (1) Heath, J. R. *Phys. Rev. B* **1989**, *40* (14), 9982–9985.
- (2) Shahbazyan, T. V.; Perakis, I. E.; Bigot, J. Y. *Phys. Rev. Lett.* **1998**, *81* (15), 3120.
- (3) Jain, P. K.; El-Sayed, M. A. *J. Phys. Chem. C* **2008**, *112* (13), 4954–4960.
- (4) Orendorff, C. J.; Sau, T. K.; Murphy, C. J. *Small* **2006**, *2* (5), 636–639.
- (5) Noguez, C. *J. Phys. Chem. C* **2007**, *111* (10), 3806–3819.
- (6) Nehl, C. L.; Hafner, J. H. *J. Mater. Chem.* **2008**, *18* (21), 2415–2419.
- (7) Barnes, W. L.; Dereux, A.; Ebbesen, T. W. *Nature* **2003**, *424* (6950), 824–830.
- (8) Lal, S.; Link, S.; Halas, N. J. *Nat. Photonics* **2008**, *1*, 641–648.
- (9) Sandrock, M. L.; Foss, C. A. *J. Phys. Chem. B* **1999**, *103* (51), 11398–11406.
- (10) Tamaru, H.; Kuwata, H.; Miyazaki, H. T.; Miyano, K. *Appl. Phys. Lett.* **2002**, *80* (10), 1826.
- (11) Rechberger, W.; Hohenau, A.; Leitner, A.; Krenn, J. R.; Lampricht, B.; Ausseneck, F. R. *Opt. Commun.* **2003**, *220* (1–3), 137–141.
- (12) Su, K. H.; Wei, Q. H.; Zhang, X.; Mock, J. J.; Smith, D. R.; Schultz, S. *Nano Lett.* **2003**, *3* (8), 1087–1090.
- (13) Atay, T.; Song, J.-H.; Nurmiikko, A. V. *Nano Lett.* **2004**, *4* (9), 1627–1631.
- (14) Jain, P. K.; Eustis, S.; El-Sayed, M. A. *J. Phys. Chem. B* **2006**, *110* (37), 18243–18253.
- (15) Romero, I.; Aizpurua, J.; Bryant, G. W.; García De Abajo, F. J. *Opt. Express* **2006**, *14* (21), 9988–9999.
- (16) Tabor, C.; Murali, R.; Mahmoud, M.; El-Sayed, M. A. *J. Phys. Chem. A* **2009**, *113* (10), 1946–1953.
- (17) Funston, A. M.; Novo, C.; Davis, T. J.; Mulvaney, P. *Nano Lett.* **2009**, *9* (4), 1651–1658.
- (18) Tabor, C.; Van Haute, D.; El-Sayed, M. A. *ACS Nano* **2009**, *3* (11), 3670–3678.
- (19) Prodan, E.; Radloff, C.; Halas, N. J.; Nordlander, P. *Science* **2003**, *302* (5644), 419–422.
- (20) Fan, J. A.; Wu, C.; Bao, K.; Bao, J.; Bardhan, R.; Halas, N. J.; Manoharan, V. N.; Nordlander, P.; Shvets, G.; Capasso, F. *Science* **2010**, *328* (5982), 1135–1138.
- (21) Hentschel, M.; Saliba, M.; Vogelgesang, R.; Giessen, H.; Alivisatos, A. P.; Liu, N. *Nano Lett.* **2010**, *10* (7), 2721–2726.
- (22) Lassiter, J. B.; Sobhani, H.; Fan, J. A.; Kundu, J.; Capasso, F.; Nordlander, P.; Halas, N. J. *Nano Lett.* **2010**, *10* (8), 3184.
- (23) Helgert, C.; Rockstuhl, C.; Etrich, C.; Menzel, C.; Kley, E. B.; uuml;nermann, A.; Lederer, F.; Pertsch, T. *Phys. Rev. B* **2009**, *79* (23), 233107.
- (24) Papasimakis, N.; Fedotov, V. A.; Fu, Y. H.; Tsai, D. P.; Zheludev, N. I. *Phys. Rev. B* **2009**, *80* (4), 041102.
- (25) Knight, M. W.; Fan, J.; Capasso, F.; Halas, N. J. *Opt. Express* **2010**, *18* (3), 2579–2587.
- (26) Fredriksson, H.; Alaverdyan, Y.; Dmitriev, A.; Langhammer, C.; Sutherland, D. S.; Zäch, M.; Kasemo, B. *Adv. Mater.* **2007**, *19* (23), 4297–4302.
- (27) Bek, A.; Vogelgesang, R.; Kern, K. *Rev. Sci. Instrum.* **2006**, *77* (4), 043703.
- (28) Esteban, R.; Vogelgesang, R.; Dorfmüller, J.; Dmitriev, A.; Rockstuhl, C.; Etrich, C.; Kern, K. *Nano Lett.* **2008**, *8* (10), 3155–3159.
- (29) Dorfmüller, J.; Vogelgesang, R.; Weitz, R. T.; Rockstuhl, C.; Etrich, C.; Pertsch, T.; Lederer, F.; Kern, K. *Nano Lett.* **2009**, *9* (6), 2372–2377.
- (30) Dorfmüller, J.; Vogelgesang, R.; Khunzin, W.; Rockstuhl, C.; Etrich, C.; Kern, K. *Nano Lett.* **2010**, *10* (9), 3596–3603.
- (31) Stockman, M. I.; Failev, S. V.; Bergman, D. J. *Phys. Rev. Lett.* **2001**, *87* (16), 167401.

- (32) Lamprecht, B.; Schider, G.; Lechner, R. T.; Ditlbacher, H.; Krenn, J. R.; Leitner, A.; Ausseneegg, F. R. *Phys. Rev. Lett.* **2000**, *84* (20), 4721.
- (33) Crozier, K. B.; Togan, E.; Simsek, E.; Yang, T. *Opt. Express* **2007**, *15*, 17482–17493.
- (34) Kneipp, K.; Wang, Y.; Kneipp, H.; Perelman, L. T.; Itzkan, I.; Dasari, R.; Feld, M. S. *Phys. Rev. Lett.* **1997**, *78* (9), 1667–1670.
- (35) Nie, S. M.; Emery, S. R. *Science* **1997**, *275* (5303), 1102–1106.
- (36) Khan, I.; Cunningham, D.; Lazar, S.; Graham, D.; Ewen Smith, W.; McComb, D. W. *Faraday Discuss.* **2006**, *132*, 171–178.
- (37) Aeschlimann, M.; Bauer, M.; Bayer, D.; Brixner, T.; Garcia de Abajo, F. J.; Pfeiffer, W.; Rohmer, M.; Spindler, C.; Steeb, F. *Nature* **2007**, *446* (7133), 301–304.
- (38) Lerosey, G.; de Rosny, J.; Tourin, A.; Fink, M. *Science* **2007**, *315*, 1120–1122.
- (39) Li, X.; Stockman, M. I. *Phys. Rev. B* **2008**, *77* (19), 195109.
- (40) Rashidi, A.; Mosallaei, H. *Phys. Rev. B* **2010**, *82* (3), 035117.
- (41) Sentenac, A.; Chaumet, P. C. *Phys. Rev. Lett.* **2008**, *101*, 013901.
- (42) Volpe, G.; Molina-Terriza, G.; Quidant, R. *Phys. Rev. Lett.* **2010**, *105* (21), 216802.
- (43) Kao, T. S.; Jenkins, S. D.; Ruostekoski, J.; Zheludev, N. I. *Phys. Rev. Lett.* **2011**, *106* (8), 085501.
- (44) Gjonaj, B.; Aulbach, J.; Johnson, P. M.; Mosk, A. P.; Kuipers, L. K.; Lagendijk, A. *Nat. Photonics* **2010**, *10*, 1038/nphoton.2011.57.